Journal of Physics Communications

PAPER

Broadband dielectric spectroscopy of Nb-doped $0.7BiFeO_3$–$0.3BaTiO_3$ ceramics

V Haronin[1], Z Yang[2], R Grigalaitis[1], I Calisir[3], J Banys[1] and D A Hall[2]

[1] Faculty of Physics, Vilnius University, LT-10226 Vilnius, Lithuania
[2] Department Materials, University of Manchester, M13 9PL, Manchester, United Kingdom
[3] Department of Chemistry, University of Liverpool, L69 7ZD, Liverpool, United Kingdom

E-mail: David.A.Hall@manchester.ac.uk

Keywords: broadband dielectric spectroscopy, perovskite solution, Re-entrant relaxor ferroelectric, ferroelectric materials, bismuth ferrite, barium titanate

OPEN ACCESS

RECEIVED
11 January 2024

REVISED
30 May 2024

ACCEPTED FOR PUBLICATION
7 June 2024

PUBLISHED
18 June 2024

Abstract

Bismuth ferrite-barium titanate (BF-BT) solid solutions are lead-free ferroelectrics that show great promise as the basis for high temperature piezoelectric transducers. This article investigates the dielectric properties of such materials using broadband dielectric spectroscopy. The study focuses on the re-entrant relaxor ferroelectric behaviour of Nb-doped BF-BT ceramics, exploring a wide frequency range from approximately 20 Hz to 30 GHz and temperature from 200 to 500 K. The results reveal the presence of thermally induced transitions between ordered and disordered states. Quantitative analysis of the dielectric dispersion is accomplished using the Cole-Cole model, modified to account for the contribution from conduction losses at low frequencies/high temperatures. This analysis revealed that the freezing temperature of the polar nanoregions is around 158 K, with an activation energy of 0.194 eV. The findings contribute to understanding the dielectric relaxation mechanisms and thermal evolution of functional properties in $BiFeO_3$-$BaTiO_3$ ceramics.

Introduction

Electrically active ceramics are widely used in different branches of industry including electronics, automation, energy conversion and storage [1]. Ferroelectrics comprise a large subgroup of such materials and are actively employed as piezoelectric sensors and actuators, tunable microwave elements, varactors etc. Until recently, lead-based ferroelectric ceramics such as $Pb(Zr,Ti)O_3$ (PZT) or $PbMg_{1/3}Nb_{2/3}O_3$-$PbTiO_3$ (PMN-PT) have dominated the market but in the last two decades the intensive search for lead-free alternatives has accelerated due to environmental concerns. Several potential candidates such as $(K,Na)NbO_3$ (KNN), $Na_{1/2}Bi_{1/2}TiO_3$ (NBT), $Ba(Zr,Ti)O_3$ (BZT) and their solid solutions with $BaTiO_3$ (BT) have been proposed, each with its own pros and cons [2, 3].

One of the viable replacements of PZT, especially for high temperature applications, is bismuth ferrite, $BiFeO_3$ (BF), which is notable due to its high Curie temperature, $T_C \approx 825$ °C [4]. Pure $BiFeO_3$ ceramics, however, are not typically regarded as promising lead-free piezoceramic candidates owing to a number of issues, including high leakage current, challenges with poling due to the high coercive field, and low piezoelectric coefficients which limits its potential usage in practical applications [4, 5]. It has been reported that the conduction mechanism for $BiFeO_3$ synthesized in air is p-type electronic [6, 7], indicating that volatilization of bismuth oxide during sintering creates oxygen vacancies and the subsequent re-oxidation taking place on cooling forms electron holes for charge compensation. Thus, the conductivity is attributed to the incorporation of excess oxygen (filling some oxygen vacancies) and the associated formation of electron holes. This can then lead to the conversion of Fe^{2+} ions to Fe^{3+} and Fe^{3+} ions to Fe^{4+}. It was also found that this p-type conduction mechanism can be shifted to n-type via reducing oxygen partial pressure during synthesis in $(Bi_{0.5}K_{0.5})TiO_3$-modified $BiFeO_3$ [8]. Furthermore, for acceptor Ca^{2+}-doped $BiFeO_3$ ceramics, it was shown that sintering in a N_2 atmosphere induced a transition from a p-type semiconductor to oxide ion conductor

[6, 9]. In spite of the fact that $BiFeO_3$ suffers from high conductivity, particularly at elevated temperatures above 400 °C, $BiFeO_3$-based piezoceramics are still suitable for high temperature transducer applications where operation at high frequencies (in the MHz range) helps to suppress the conduction losses [10].

Control of the conductivity in piezoceramics is conventionally achieved by doping with either iso- and alio-valent cations or forming solid solutions with another perovskite end-members such as $BaTiO_3$. In the case of the $BiFeO_3$-$BaTiO_3$ (BF-BT) solid solution system, it was found that a minor amount of dopant is required in order to reduce the high leakage current [11]. Leontsev *et al* reported that a small amount of MnO_2 addition in BF-BT ceramics can improve the ferroelectric properties and also reduce the electrical conductivity down to the level required to observe saturated polarization hysteresis loops with relatively low coercive field [12]. A similar effect can be achieved by donor type Nb^{5+}-substitution on the B-site in BF-BT. It was discovered that Nb^{5+} substitution for Fe^{3+} can significantly decrease electronic conductivity and improve temperature stability in BF-BT solid solutions [13], enhance electric breakdown strength and energy storage characteristics [14]. One of the intriguing properties found in Nb-doped BF-BT is that it shows re-entrant relaxor ferroelectric behaviour upon cooling [15], as similarly reported in other pseudo-binary solid solution systems with perovskite ($BaTiO_3$-$BiScO_3$) [16], and tungsten bronze ($Sr_2NaNb_5O_{15}$) structures [17].

Phase transitions in ferroelectric materials are typically characterized by a sharp transition from a disordered high-symmetry phase to a more ordered low-symmetry phase as the temperature decreases. However, some materials exhibit unusual sequences. In relaxor ferroelectrics, for example, there is an intermediate *ergodic relaxor* phase between the high-temperature disordered phase and the low-temperature ordered phase. In other materials, upon further cooling after the ordered phase, a re-entrant disordered phase can occur that loses the order of the intermediate phase. This re-entrant phase can have lower entropy than the ordered phase, indicating that the order parameter does not fully describe the order–disorder processes [18].

To investigate the re-entrant relaxor behaviour and its origin in ferroelectric ceramics, the initial consideration must be to check whether there are inhomogeneities related to compositional segregation or disorder in the material since observable phase transitions such as the Curie temperature, T_C, or dielectric maximum temperature, T_m, could be associated with the chemically different macroscopic regions of the material. Other types of interfacial inhomogenities must be also considered when examining the re-entrant behaviour of polycrystalline ceramics, such as those at grain boundaries or ceramic/electrode interfaces, which often lead to Maxwell–Wagner type dielectric response with a distinctive dielectric dispersion [16, 18]. These types of extrinsic dielectric contributions, which can each be responsible for dielectric anomalies, must be distinguished in order to reveal true re-entrant behaviour. This work aims to investigate the dielectric properties of Nb-doped 0.7BF−0.3BT ceramics with consideration of re-entrant relaxor ferroelectric behavior by covering wide frequency (from Hz to GHz) and temperature (200 to 500 K) ranges. Our study explores the low-temperature relaxor-like dispersion in order to complement the structural and dielectric data published previously [14, 15].

Materials and methods

Both pure ($0.7BiFeO_3$–$0.3BaTiO_3$) and Nb-doped ($0.7BiFe_{0.995}Nb_{0.005}O_3$–$0.3BaTiO_3$) ceramics were synthesized by the solid-state reaction method using Bi_2O_3 (99%), Fe_2O_3 (99%), $BaCO_3$ (99%), TiO_2 (99%) and Nb_2O_5 (99.99%) powders (Sigma-Aldrich, Gillingham, UK). The mixed/milled powders were calcined at 800 °C for 4 h and sintered at 1010 °C for 3 h to obtain ceramic samples having a relative density greater than 95% [15]. X-ray diffraction data for these samples indicated a single phase perovskite structure with rhombohedral R3c crystal symmetry [15]. Silver contacts were subsequently applied on both sides of the disk-shaped sample to create planar capacitor structures.

Dielectric spectra of the BF-BT ceramics were measured in a broad frequency range from 20 Hz to 30 GHz at temperatures from 200 to 500 K. This wide range of frequencies was covered using three different dielectric measurement instruments (i) a HP4284A LCR meter was used for the 20 Hz to 1 MHz frequency band, to measure capacitance and loss tangent and values of dielectric permittivity were calculated using the planar capacitor formula; (ii) the 1 MHz to 1 GHz frequency band was covered by a vector network analyser, Agilent 8714ET measuring the complex reflection coefficient of a short-circuited sample placed at the end of coaxial line; (iii) measurements between 25 and 40 GHz were carried out by inserting a thin rectangular rod into the waveguide's centre. The scalar reflection and transmission coefficients were measured in a waveguided system using a scalar network analyser, Elmika 2400. The complex dielectric permittivity for methods (ii) and (iii) was calculated by variations of a multimode capacitor model for circular and rectangular waveguides respectively. More details are published in our recent papers [19, 20]. In this case, temperature was measured using a Keithley Integra 2700 connected to a T-type thermocouple or 100 ohm platinum resistance thermometer (4W-RTD).

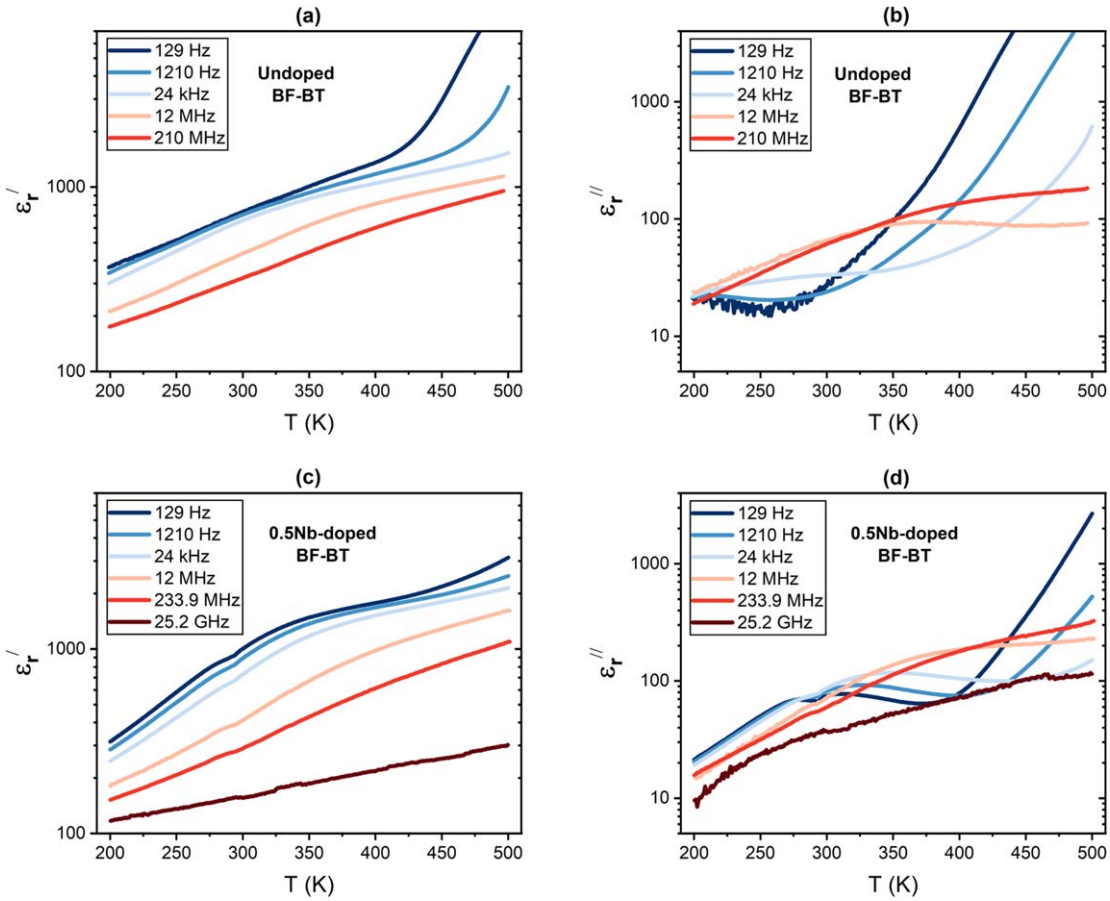

Figure 1. Temperature dependence of real, ε_r', and imaginary, ε_r'', parts of complex dielectric permittivity of (a)–(b) undoped and (c)–(d) 0.5Nb-doped $BiFeO_3$–$BaTiO_3$ (BF-BT) ceramics, measured over a broad range of frequencies.

Results and discussion

The temperature dependencies of the real and imaginary parts of the complex dielectric permittivity of both pure (undoped BF-BT) and Nb-doped (BF-BT-0.5Nb) BF-BT ceramics are shown in figure 1. In both cases, the real part exhibits a strong frequency dependence and rises significantly on heating from 200 K, with a 'shoulder' at 350 K, followed by a more gradual increase prior to the dielectric maximum associated with the Curie point at 740 K [15]. A frequency-dependent maximum is evident in the imaginary part of permittivity for the Nb-doped ceramic over the temperature range from 270 to 400 K, which shifts toward higher temperatures with increasing frequency and is correlated with the anomalous increase in rhombohedral distortion with rising temperature in this range [15]. Similar relaxation effects were also present, although less pronounced, for the undoped BF-BT. Usually, such thermally activated dielectric behavior is attributed to disordered solids like dipolar glasses or relaxor ferroelectric (RF) [21–23] which have a broad distribution of relaxation times caused by polar nano regions (PNRs) or frustrated dipoles. The exponential rise in ε_r'' with increasing temperature above 400 K, shown in figures 1(b) and (d), is attributed to increasing conductivity, σ, due to the evident inverse dependence on frequency in this temperature range [24].

In contrast to the majority of relaxor ferroelectrics, where relaxor-type dielectric dispersion occurs at higher temperatures than the phase transition to the ferroelectric state (if it occurs), in this case the ferroelectric phase occurs at a higher temperature than that of the RF state. Such a sequence of transitions is characteristic of re-entrant phenomena, as noted above, and usually occurs by breaking an ordered state into a disordered one or due to the coexistence of ordered and disordered states at different scales [25–27]. It can be challenging to interpret such behavior, since similar types of dielectric dispersion could originate due to different processes such as domain wall relaxation or charge accumulation at interfaces of grains. Nevertheless, the previous results suggest that these effects are associated with disruption of ferroelectric ordering at lower temperatures, perhaps due to off-polar displacements of the Bi^{3+} ions [15, 28–30]. The following analysis focuses on the analysis of dielectric relaxation in the Nb-doped BF-BT ceramics, in which the strength of the relaxation was most clearly evident.

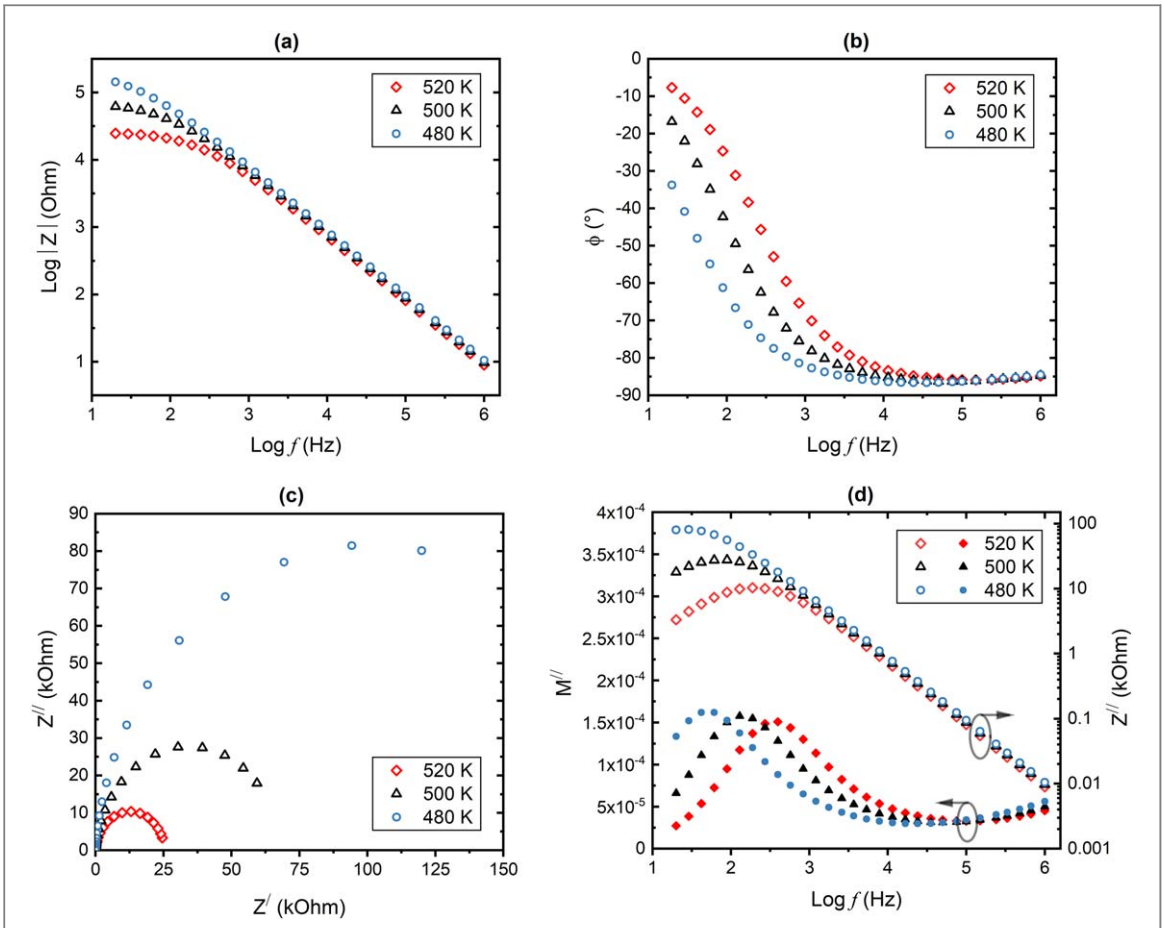

Figure 2. Impedance spectroscopy data for Nb-doped BF-BT ceramics presented in several different formats to illustrate the transition from a predominantly capacitive ($\phi < -45°$) to resistive ($\phi > -45°$) electrical response at low frequencies and higher temperatures. Bode plots for (a) impedance magnitude and (b) phase angle; (c) complex impedance plot; (d) bode plots for imaginary parts of complex modulus and impedance.

At sufficiently high temperatures and low frequencies, the in-phase real (resistive) component of the complex impedance, Z′, begins to dominate over the imaginary (capacitive) part, Z″, and the phase angle, ϕ, shifts from -90° towards zero; these effects are illustrated by the Bode plots presented in figures 2(a) and (b). In figure 2(c), the extrapolated intercept of the semi-circular arc with the real, Z′, axis corresponds to the resistance of the equivalent circuit represented by a parallel C-R network, which is inversely proportional to conductivity and dielectric loss according to equation (1). It is evident that the resistance decreases while the conductivity and dielectric loss increase with increasing temperature. Such an equivalent circuit also corresponds to contributions from the bulk (grain) permittivity and conductivity, with reduction in the resistance at higher temperatures being driven by thermal activation of charge carriers [14]. The Bode plots for the imaginary parts of complex impedance and modulus, Z″ and M″ respectively (figure 2(d)), exhibit peaks that overlap approximately in the peak frequency, indicating good electrical homogeneity [6].

To gain more information about the dielectric relaxation characteristics, the frequency-dependent complex permittivity data, obtained at various temperatures, are plotted in figure 3. For analysis of the dielectric spectra, an empirical Cole-Cole equation [31], modified to include the conduction contribution to loss at low frequencies/high temperatures [32], was used to model the experimental complex permittivity data, yielding estimates of the dielectric parameter values. Simultaneously, the Levenberg–Marquardt algorithm based non-linear least square method was used in the fitting procedure. OriginLab software was employed to implement these algorithms for fitting the experimental data with the following formula:

$$\varepsilon^*(\omega) = \sum_{i=1}^{n} \varepsilon_{\infty_i} + \frac{\Delta\varepsilon_i}{1 + (i\omega\tau_i)^{1-\alpha_i}} + \frac{\sigma}{2\pi i f^k} \tag{1}$$

where ε_∞ is the dielectric constant at infinite frequency, $\Delta\varepsilon$ is the strength of the relaxation process, ω is the angular frequency, τ is the mean relaxation time and α is a parameter that describes the broadness of the dispersion. The integer, n, represents the number of relaxation processes present in the dielectric spectra at a given temperature and varies from 1 to 2 depending on the complexity of the dispersion. The third part of this

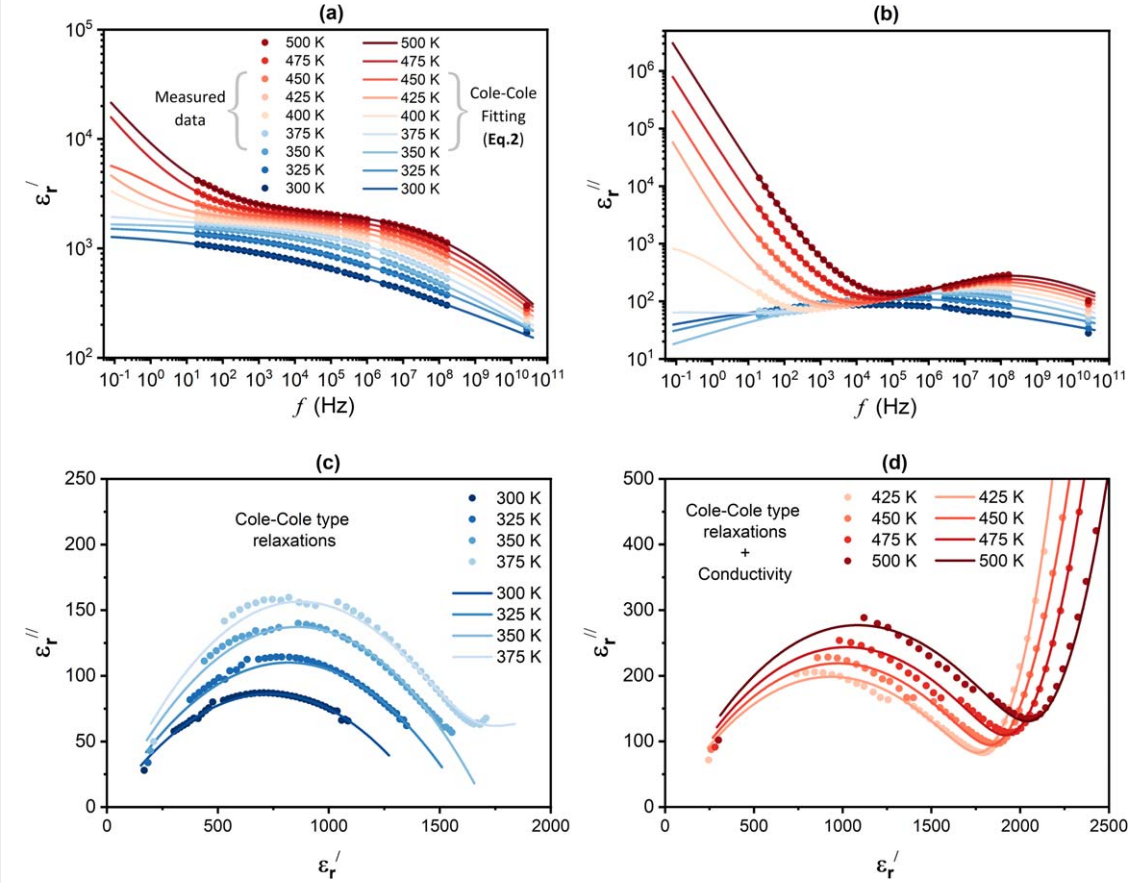

Figure 3. Frequency dependencies of the (a) real and (b) imaginary parts of dielectric permittivity of 0.5Nb-$BiFeO_3$–$BaTiO_3$ ceramics at different temperatures. Lines show the best fits of experimental data points according to equation (2). Complex permittivity (Cole-Cole) plots for (c) low and (d) high temperature ranges, illustrating the thermally-activated conduction losses.

expression represents the conduction contribution to the imaginary part of permittivity, modified with an additional fitting parameter, *k*.

Dielectric data in the 300–350 K temperature region clearly show a single dispersion in the whole measured frequency range, illustrated in figures 3(a) and (b). It is evident that this dispersion broadens toward lower frequencies on cooling but still retains a symmetric form and was fitted using equation (2) with a single relaxation process (n = 1). The single dielectric relaxation mechanism is also indicated by the semi-circular form of the Cole-Cole plot for the complex permittivity shown in figure 3(c). At temperatures between 350 K and 400 K, an additional low-frequency lossy process starts to appear in the dielectric dispersion curves, illustrated in figures 3(b) and (d), which is attributed to the effects of increasing electrical conductivity as noted above. For temperatures above 450 K a slight increase in the real part of the dielectric permittivity starts to accompany the rising dielectric losses. This effect can be attributed to the effect of accumulation of localized electrical charges at the interfaces between grains and their migration at elevated temperatures, usually described as Maxwell Wagner relaxation [33].

For higher temperatures above 400 K, both the low- and high-frequency dispersions remain active, while their evolution with temperature shows the same trend and the same procedure can be employed for fitting their frequency dependencies. However, more careful analysis indicated weak imperfections of the fit in the 10^4-10^6 Hz frequency range (in the vicinity of the minimum of the dielectric losses) and the best fits were obtained by including a 2nd Cole-Cole process. Since this relaxation is very weak and highly overlapped with the high-frequency relaxation, it is not possible to analyze the mechanism in more depth. The fitted *k* values (1.001 at 500 K, 1.006 at 475 K, 1.012 at 450 K and 1.069 at 425 K) were generally close to 1, confirming the dominance of the conduction contribution to ε_r'' at higher temperatures.

As noted above, the high-frequency dispersion shows substantial thermal evolution, and we were able to extract the temperature dependencies of the parameters of the respective Cole-Cole process (figure 4). The parameter α, which represents the broadness of the dielectric dispersion, increases linearly from about 0.68 at 500 K to 0.85 at room temperature. This shows that in this system there is a broad distribution of polar entities having different relaxation times even at the highest temperature (500 K). This picture clearly deviates from

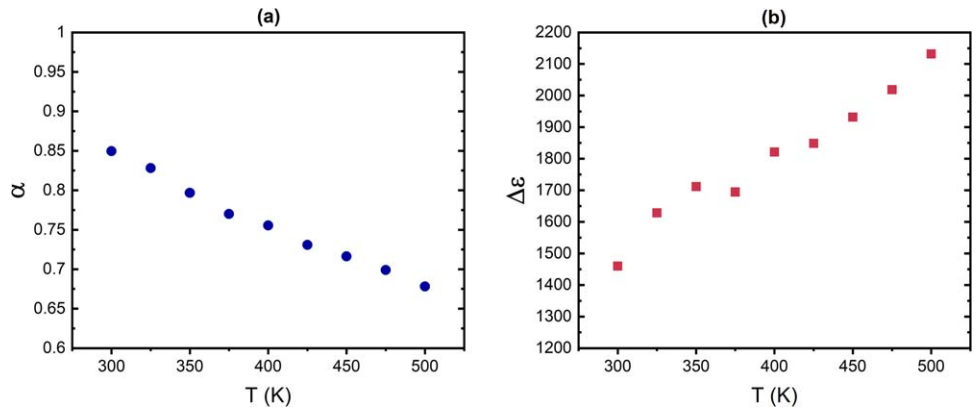

Figure 4. Temperature dependence of (a) dielectric dispersion parameter, α, and (b) strength of the relaxation, $\Delta\varepsilon$, in 0.5Nb-$BiFeO_3$–$BaTiO_3$ ceramics.

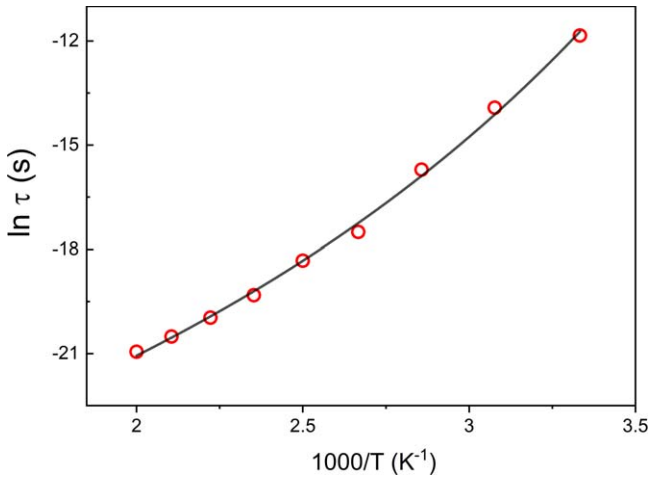

Figure 5. Inverse temperature dependence of the mean relaxation time in 0.5Nb-$BiFeO_3$–$BaTiO_3$ ceramics.

Debye-type dispersion ($\alpha = 0$) where only one type of dipole causing one relaxation time exists. Another parameter, the strength of the relaxation, $\Delta\varepsilon$, clearly shows the opposite trend with respect to temperature compared with parameter α. This implies a decreasing contribution to the total dielectric permittivity of this relaxation process on cooling.

The inverse temperature dependence of the mean relaxation time is shown In figure 5. The data presented correspond to fitting results obtained by approximating the frequency dependences of the dielectric permittivity by the Cole-Cole formula, in combination with the Vogel–Fulcher-Tamman law which is commonly used to describe the relaxation dynamics in inhomogeneous systems such as relaxor ferroelectrics [34]:

$$\tau = \tau_0 \exp\left(\frac{E}{k(T - T_f)}\right), \tag{2}$$

where τ_0 is the relaxation time for $T \to \infty$, E is the activation energy, k is the Boltzmann constant and T_f represents the temperature at which the relaxation process 'freezes'.

The fitted curve exhibits a good fit to the experimental data with the corresponding parameters, $\tau_0 = 1.73 \times 10^{-12}$ s, $T_f = 158 \pm 16$ K and $E = 0.194$ eV. From the obtained results, it is evident that the average relaxation time increases with reducing temperature and clearly deviates from the Arrhenius law ($T_f = 0$). This means that this relaxation process is similar to the one typically seen in dipolar glasses or relaxor ferroelectrics having a broad distribution of relaxation times [21–23]. The activation energy also lies in the range typically obtained for these systems [22].

Conclusions

In summary, broadband dielectric spectroscopy measurements conducted on 0.7BF-0.3BT ceramics doped with 0.5% Nb reveal evidence for a low-temperature relaxation mechanism reminiscent of relaxor ferroelectrics or dipolar glass relaxations at temperatures in the range 250 to 500 K, well below the ferroelectric phase transition at 740 K. Analysis employing the Cole-Cole relaxation model reveals a broad distribution of relaxation times, with a distinct divergence in mean relaxation time. Particularly interesting is the conformity to the Vogel–Fulcher-Tamman law, with a freezing temperature of 158 K and a corresponding activation energy of 0.194 eV, consistent with those of other relaxor ferroelectric materials. These findings highlight the unique characteristics of Nb-doped BF-BT ceramics, offering valuable insights into the re-entrant relaxor ferroelectric behaviour.

Acknowledgments

DAH thanks the EPSRC for support through grants EP/S028978/1 and EP/V053183/1.

Data availability statement

The data cannot be made publicly available upon publication because they are not available in a format that is sufficiently accessible or reusable by other researchers. The data that support the findings of this study are available upon reasonable request from the authors.

ORCID iDs

V Haronin https://orcid.org/0000-0003-3782-7629
Z Yang https://orcid.org/0000-0002-1202-9551
R Grigalaitis https://orcid.org/0000-0001-7007-2024
I Calisir https://orcid.org/0000-0002-4199-9127
J Banys https://orcid.org/0000-0003-3507-0343
D A Hall https://orcid.org/0000-0002-7541-457X

References

[1] Setter N and Waser R 2000 Electroceramic materials *Acta Mater.* **48** 151–78
[2] Rödel J and Li J F 2018 Lead-free piezoceramics: Status and perspectives *MRS Bull.* **43** 576–80
[3] Rödel J *et al* 2009 Perspective on the development of lead-free piezoceramics *J. Am. Ceram. Soc.* **92** 1153–77
[4] Catalan G and Scott J F 2009 Physics and applications of bismuth ferrite *Adv. Mater.* **21** 2463–85
[5] Rojac T *et al* 2014 $BiFeO_3$ ceramics: processing, electrical, and electromechanical properties *J. Am. Ceram. Soc.* **97** 1993–2011
[6] Masó N and West A R 2012 Electrical properties of Ca-doped $BiFeO_3$ ceramics: from p-type semiconduction to oxide-ion conduction *Chem. Mater.* **24** 2127–32
[7] Schrade M, Masó N, Perejón A, Pérez-Maqueda L A and West A R 2017 Defect chemistry and electrical properties of $BiFeO_3$ *J. Mater. Chem.* C **5** 10077–86
[8] Wefring E T, Einarsrud M A and Grande T 2015 Electrical conductivity and thermopower of (1-X) $BiFeO_3$-x$Bi_{0.5}K_{0.5}TiO_3$ (x = 0.1, 0.2) ceramics near the ferroelectric to paraelectric phase transition *Phys. Chem. Chem. Phys.* **17** 9420–8
[9] Li L, Kler J, West A R, De Souza R A and Sinclair D C 2021 High oxide-ion conductivity in acceptor-doped Bi-based perovskites at modest doping levels *Phys. Chem. Chem. Phys.* **23** 11327–33
[10] Stevenson T *et al* 2015 Piezoelectric materials for high temperature transducers and actuators *J. Mater. Sci., Mater. Electron.* **26** 9256–67
[11] Calisir I and Hall D A 2018 Chemical heterogeneity and approaches to its control in $BiFeO_3$–$BaTiO_3$ lead-free ferroelectrics *J. Mater. Chem.* C **6** 134–46
[12] Leontsev S O and Eitel R E 2009 Dielectric and piezoelectric properties in Mn-modified (1−x)$BiFeO_3$–x $BaTiO_3$ ceramics *J. Am. Ceram. Soc.* **92** 2957–61
[13] Chaudhary P, Shukla R, Dabas S and Thakur O P 2021 Enhancement of structural, magnetic, dielectric, and transport properties of Nb substituted 0.7$BiFeO_3$-0.3$BaTiO_3$ solid solution *J. Alloys Compd.* **869** 159228
[14] Yang Z, Wang B, Li Y and Hall D A 2022 Enhancement of nonlinear dielectric properties in $BiFeO_3$–$BaTiO_3$ ceramics by Nb-doping. *Materials* **15** 2872
[15] Yang Z *et al* 2023 Re-entrant relaxor ferroelectric behaviour in Nb-doped $BiFeO_3$-$BaTiO_3$ ceramics *J. Mater. Chem.*C **11** 2186–95
[16] Guo H Y, Lei C and Ye Z-G 2008 Re-entrant type relaxor behavior in (1−x)$BaTiO_3$–x$BiScO_3$ solid solution *Appl. Phys. Lett.* **92** 172901
[17] Torres-Pardo A, Jiménez R, González-Calbet J M and García-González E 2011 Structural effects behind the low temperature nonconventional relaxor behavior of the $Sr_2NaNb_5O_{15}$ bronze *Inorg. Chem.* **50** 12091–8
[18] Bokov A A and Ye Z 2016 Reentrant phenomena in relaxors *Nanoscale Ferroelectrics and Multiferroics* (Wiley) 729–64
[19] Svirskas Š *et al* 2020 Broad-band measurements of dielectric permittivity in coaxial line using partially filled circular waveguide *Rev. Sci. Instrum.* **91** 035106
[20] Zamaraite I *et al* 2022 Computational electromagnetic analysis of partially-filled rectangular waveguide at X-band frequencies *Nonlinear Anal. Model. Control* **27** 1150–67
[21] Grigalaitis R, Banys J, Kania A and Slodczyk A 2005 Distribution of relaxation times in PMN single crystal *J. Phys. IV* **128** 127–31

[22] Macutkevic J, Banys J, Grigalaitis R and Vysochanskii Y 2008 Asymmetric phase diagram of mixed $CuInP_2(S_xSe_{1-x})_6$ crystals *Phys. Rev.* B **78** 064101
[23] Banys J, Grigalaitis R, Mikonis A, Macutkevic J and Keburis P 2009 Distribution of relaxation times of relaxors: comparison with dipolar glasses *Phys. Status Solidi C* **6** 2725–30
[24] Härdtl K H 1982 Electrical and mechanical losses in ferroelectric ceramics *Ceram. Int.* **8** 121–7
[25] Bharadwaja S S N *et al* 2011 Critical slowing down mechanism and reentrant dipole glass phenomena in $(1-x)BaTiO_{3-x}BiScO_3$ ($0.1 \leqslant x \leqslant 0.4$): the high energy density dielectrics *Phys. Rev.*B **83** 024106
[26] Pokharel B, Shrestha L, Ariga K and Pandey D 2018 Demonstration of reentrant relaxor ferroelectric phase transitions in antiferroelectric-based $(Pb_{0.50}Ba_{0.50})$ ZrO_3 ceramics *Energies* **11** 850
[27] Surampalli A, Egli R, Prajapat D, Meneghini C and Reddy V R 2021 Reentrant phenomenon in the diffuse ferroelectric $BaSn_{0.15}Ti_{0.85}O_3$: local structural insights and first-order reversal curves study *Phys. Rev.*B **104** 184114
[28] Singh A, Moriyoshi C, Kuroiwa Y and Pandey D 2013 Visualization of Bi3+ off-centering in the average cubic structure of $(Ba_{0.7}0Bi_{0.30})(Ti_{0.70}Fe_{0.30})O_3$ at the electron density level *Appl. Phys. Lett.* **103** 121907
[29] Singh A, Moriyoshi C, Kuroiwa Y and Pandey D 2012 Evidence for diffuse ferroelectric phase transition and cooperative tricritical freezing of random-site dipoles due to off-centered Bi^{3+} ions in the average cubic lattice of $(Ba_{1-x}Bi_x)(Ti_{1-x}Fe_x)O_3$ *Phys. Rev.*B **85** 064116
[30] Kuroiwa Y *et al* 2020 Piezoelectricity in perovskite-type pseudo-cubic ferroelectrics by partial ordering of off-centered cations *Commun. Mater.* **1** 71
[31] Cole K S and Cole R H 1941 Dispersion and absorption in dielectrics I. Alternating current characteristics *J. Chem. Phys.* **9** 341–51
[32] Srivastava S *et al* 2015 Synthesis of zinc oxide (ZnO) nanorods and its phenol sensing by dielectric investigation *J. Alloys Compd.* **644** 597–601
[33] Wang T *et al* 2017 Dielectric relaxation and Maxwell-Wagner interface polarization in Nb_2O_5 doped $0.65BiFeO_3$-$0.35BaTiO_3$ ceramics *J. Appl. Phys.* **121** 084103
[34] Ngai K L 2011 *Relaxation and Diffusion in Complex Systems* (Springer) (https://doi.org/10.1007/978-1-4419-7649-9)